Theory of inelastic collisions between low-lying excited- and ground-state Ne atoms

James S. Cohen
Theoretical Division, Los Alamos Scientific Laboratory, University of California, Los Alamos, New Mexico 87545

Lee A. Collins*
Joint Institute for Laboratory Astrophysics, University of Colorado and National Bureau of Standards, Boulder, Colorado 80309

Neal F. Lane
Department of Physics, Rice University, Houston, Texas 77001
(Received 30 November 1977)

A quantum-mechanical study of low-energy inelastic collisions of excited- and ground-state Ne atoms has been undertaken. Close-coupling calculations of cross sections for the transitions $^1P_1 \rightarrow {}^3P_1$, $^1P_1 \rightarrow {}^3P_2$, $^3P_1 \rightarrow {}^3P_2$, and $^3P_0 \rightarrow {}^3P_2$ have been performed at collision energies below 3 eV. All cross sections exhibit a rapid falloff at low energies, reflecting barriers and repulsive walls present in the potential curves. Spin-orbit coupling is assumed to be the transition mechanism. Comparison with experimental data suggests that neglected rotational coupling might be important for some of the quite weak transitions at energies below about 0.1 eV.

I. INTRODUCTION

The theory of low-energy ($\lesssim$100 eV) inelastic atom-atom and ion-atom scattering has received considerable attention over the past decade or so, and significant progress has been made in understanding the basic mechanisms. It is well known that for cases of resonant symmetric charge or excitation transfer, where an actual electronic transition is not required, the cross section can be quite large (i.e., comparable with elastic) at low energies.[1] Even in cases of resonant or near-resonant asymmetric charge or excitation transfer, where an electronic transition is required, the cross section can still be very large at low energies, provided the perturbation which provides the electronic coupling is sufficiently strong.[2] Massey's adiabatic criterion,[3] suitably generalized to apply at finite internuclear separations, is useful as a qualitative indication of where, in energy, the cross section is likely to be large. It is generally found that appreciable low-energy cross sections arise from molecular "curve crossings" or "avoided crossings." Under very restrictive conditions a remarkable simplification of the collision problem is made possible by the "Stueckelberg-Landau-Zener" (SLZ) approximation.[4] Because it is so easy to apply, the approximation is often stretched beyond its range of applicability; it can give exceedingly poor results. Several investigators have made careful studies of the SLZ and related approximations,[5-9] in some cases by comparing approximate and exact results for well-defined model problems.[9] In addition to direct applications of the theoretical methods to particular collision processes, a number of more fundamental theoretical studies have been made which shed light on such questions as the nature of the "diabatic" state,[7,10-12] proper treatment of electron "translation factors" in imposing scattering boundary conditions,[13] and the consideration of dynamic symmetries in analyzing curve crossings.[14]

Applications to inelastic collisions between excited- and ground-state rare-gas atoms, other than helium,[9,15] have not previously been made in spite of the importance of such processes in the dense-gas environment most appropriate to excimer lasers.[16] Significant progress has recently been made in the understanding of the electron-bombarded dense-rare-gas systems by means of careful time-dependent spectroscopic measurements.[17,18] However, in attempting to determine a consistent set of rates for the various processes that control time development of the system, one has at present very little theoretical guidance. The processes of inelastic excitation transfer, or "mixing," in collisions of excited- and ground-state atoms are important since they play a role in determining the populations of gas atoms present in particular excited states, for example, and thereby influence subsequent reactions leading to excimer formation. An earlier study was performed of resonant excitation and charge transfer in Ne.[19]

We report here a theoretical calculation of cross sections for several transitions induced by collisions of excited- and ground-state neon atoms. Neon has not been experimentally studied as extensively as the other rare gases, but has the advantage that a theoretical treatment of the molecular structure of Ne_2^* has been carried out for

a number of excited states.[20] Moreover, it is the lightest of the "heavy" rare gases, so that the spin-orbit interaction, though important, may still be viewed as a moderate perturbation. In Sec. II we review the molecular structure of Ne_2^*. In Sec. III, the quantum-mechanical theory of atom-atom scattering is reviewed very briefly and the approximations made in the present study are described. In Sec. IV, the numerical procedures are outlined, and in Sec. V, the results of the calculations are presented and discussed.

II. MOLECULAR STRUCTURE OF Ne_2^*

A qualitative description of the ground and excited states of homonuclear rare-gas molecules and the corresponding molecular ions has been given by Mulliken.[21] In the molecular-orbital description, the $^1\Sigma_g^+$ ground state is described approximately by the configuration (LCAO notation)

$$\cdots(\sigma_g ns)^2(\sigma_u ns)^2(\sigma_g np)^2(\pi_u np)^4(\pi_g np)^4(\sigma_u np)^2$$

arising from two closed-shell ground-state atoms, each described approximately by the atomic configuration $\cdots(ns)^2(np)^6$, where $n = 2, 3, 4, 5$ for Ne, Ar, Kr, and Xe, respectively, and where lower-lying orbitals are taken to be fully occupied. The low-lying excited molecular states correspond to the promotion of one of these six molecular orbitals. The excited electron is expected to be of Rydberg character, and the corresponding potential energy curve, consequently, will resemble that of the "parent" molecular ion (or "ion core") to which this excited electron is bound (though the well depths are generally somewhat smaller). Two low-lying states of the molecular ion result from the removal of an electron from either of the antibonding orbitals $\sigma_u np$ or $\pi_g np$; these states are traditionally designated as $A\,^2\Sigma_u^+$ and $B\,^2\Pi_g$, respectively. Thus, depending on the symmetry of the excited electron, a number of $^{1,3}\Sigma_{g,u}$ and $^{1,3}\Pi_{g,u}$ states are possible. The spin-orbit interaction is, of course, important for all the heavy rare gases. The appropriate designation of the states, including this effect, is $0_{g,u}^{\pm}$, $1_{g,u}$, $2_{g,u}$, etc., where 0, 1, 2 are values of Ω, the projection of the total angular momentum (spin and orbital) on the internuclear axis, and where the + and − reflection symmetries for $\Omega = 0$ do not in general correspond to degenerate states. *Ab initio* studies of the ground states for various rare-gas molecules have been performed; however, theoretical information on the excited states is scarce.

Cohen and Schneider have calculated wave functions, energies, spectroscopic parameters, and radiative lifetimes for a number of the excited states of diatomic neon.[20,22] They applied a generalized valence-bond variational procedure, using a Slater-orbital basis set which is double zeta plus polarization for the valence orbitals and single zeta for the core orbitals including $2s$. The orbital exponents were optimized at several internuclear separations. In the configuration-interaction calculation, typically about 30 configurations, including the most important single and double excitations, were used. The spin-orbit coupling matrix elements were taken to be independent of internuclear separation, and were determined semiempirically using atomic spectral data. It was argued that the most important spin-orbit effect arises from the ion cores, which do not overlap appreciably except at very small internuclear separations. The *ab initio* calculations were carried out ignoring the spin-orbit interaction, thus obtaining "ΛS states"; the potential energy curves for the first eight states are shown in Fig. 1. When the spin-orbit interaction is included, significant Σ-Π and singlet-triplet mixing occurs, and the potential energy curves corresponding to the Ω states exhibit features (e.g., avoided crossings) not present in the ΛS curves. The curves for $\Omega = 0$ and 1 are given in Fig. 2. For later reference, we illustrate in Table I the ΛS-state mixing and the separated-atoms correlation for each of the Ω states.

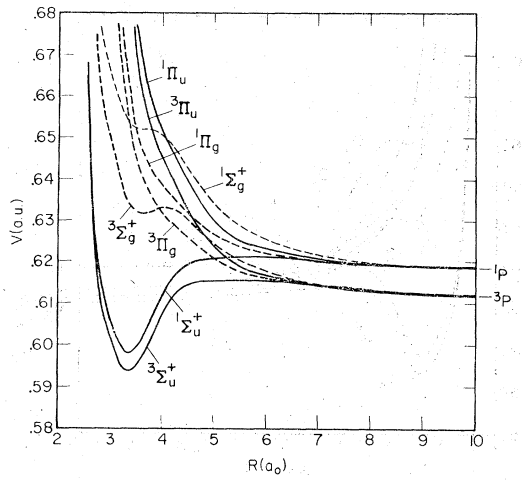

FIG. 1. Potential curves of Ne_2^* not including spin-orbit interaction (ΛS representation).

Characteristic features of the potential curves shown in Fig. 2, which influence the inelastic cross sections in the most direct manner, are the barriers present in the lowest $0_u^-(^3P_2)$, $0_u^+(^3P_1)$, $0_u^+(^1P_1)$, and $1_u(^3P_2)$ curves, the replusive nature of the other curves, and avoided crossings between the $0_u^+(^3P_1)$ and $0_u^+(^1P_1)$ curves, and between the corresponding g curves.

The repulsive nature of all the curves for $R \gtrsim 5a_0$

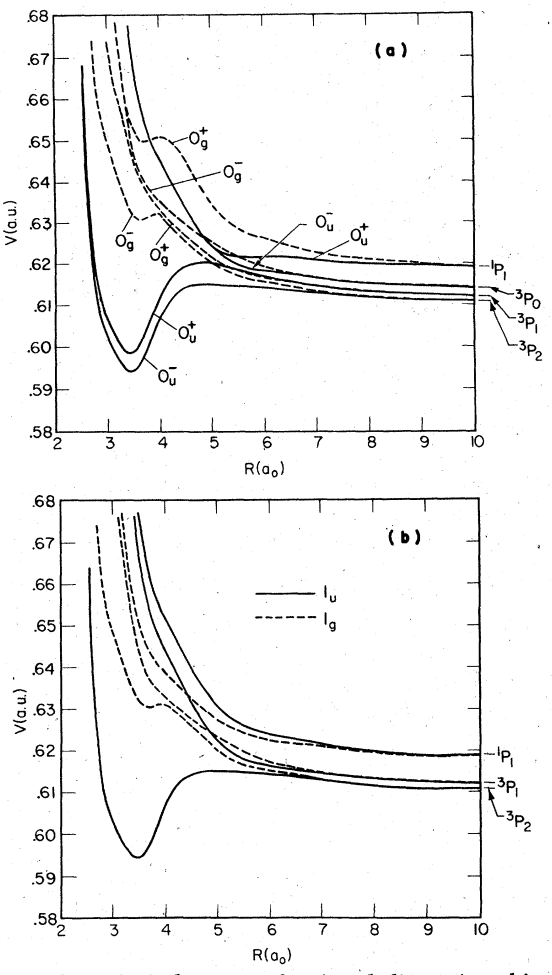

FIG. 2. Potential curves of Ne_2^* including spin-orbit interaction for (a) $\Omega=0$ and (b) $\Omega=1$.

results in inelastic cross sections which are very small at low energies, but which rise rapidly as the energy is increased. The avoided crossing between the curves for $0_u^+(^3P_1)$ and $0_u^+(^1P_1)$ results in an enhanced $^1P_1 \rightarrow {}^3P_1$ cross section, which for energies $\gtrsim 0.1$ eV is larger than all others considered here.

III. THEORY OF Ne*-Ne COLLISION PROCESSES

The theoretical framework employed here is essentially that of coupled perturbed-stationary states.[1,23] The time-independent wave function of the diatomic system $\Psi(\vec{r},R)$ is expanded in a basis set of electronic functions $\psi_\alpha(\vec{r},R)$ which may reflect some degree of adiabatic molecular formation.[24] The expansion takes the form

$$\Psi(\vec{r},\vec{R})=\sum_\alpha F_\alpha(\vec{R})\psi_\alpha(\vec{r},R)\,, \tag{1}$$

where the coefficients $F_\alpha(\vec{R})$ play the role of nuclear wave functions.[25,26] The coupled equations which result from substitution of this expansion into the Schrödinger equation may be written (atomic units are used throughout)

$$[-(1/2\mu)\nabla_R^2-\mathcal{E}]F_\alpha(\vec{R})$$
$$=\sum_{\alpha'}[-\langle\alpha|H_e|\alpha'\rangle+(1/\mu)\langle\alpha|\nabla_R|\alpha'\rangle\cdot\nabla_R$$
$$+(1/2\mu)\langle\alpha|\nabla_R^2|\alpha'\rangle]F_{\alpha'}(\vec{R}), \tag{2}$$

where μ and $\mathcal{E}$ are the reduced mass and total energy, respectively, and H_e is the electronic Hamiltonian including nuclear-repulsion terms; it is assumed that ∇_R and ∇_R^2 in the matrix elements do not operate outside the integrals. If a completely adiabatic (i.e., Born-Oppenheimer) basis is chosen, then H_e is diagonal, and all coupling between different states arises from the relative motion of the nuclei. Many of these matrix elements, however, are difficult to calculate accurately, even for rather simple diatomic systems. As a compromise, investigators often seek an intermediate nonadiabatic basis set which exhibits relatively smooth variation with R, where coupling via H_e dominates that resulting from relative nuclear motion.[7-12]

TABLE I. ΛS mixing and separated-atoms correlation.

State	ΛS Mixing			Separated-atoms correlation		
$0_{g,u}^-$	$^3\Sigma_{g,u}^+$	$^3\Pi_{g,u}$		$^3P_2$	$^3P_0$	
$0_{g,u}^+$	$^3\Pi_{g,u}$	$^1\Sigma_{g,u}^+$		$^3P_1$	$^1P_1$	
$1_{g,u}$	$^3\Sigma_{g,u}^+$	$^3\Pi_{g,u}$	$^1\Pi_{g,u}$	$^3P_2$	$^3P_1$	$^1P_1$
$2_{g,u}$	$^3\Pi_{g,u}$			$^3P_2$		

In the Ne_2 system, we make use of the approximate wave functions of Cohen and Schneider. As an intermediate nonadiabatic basis set, we choose the states $|n\Lambda S\rangle$ which diagonalize the electronic Hamiltonian neglecting the spin-orbit interaction, where n stands for all quantum numbers in addition to ΛS necessary to specify the state. These states are then coupled by the spin-orbit interaction, approximated in the semiempirical manner of Cohen and Schneider.[20] It is assumed that the additional coupling via the nuclear motion, i.e., the ∇_R and ∇_R^2 matrix elements, is less effective in inducing transitions, and the latter is ignored in the present study. Therefore, the expansion of Eq. (1) becomes

$$\Psi(\vec{r},\vec{R})=\sum_{n\Lambda S} F_{n\Lambda S}(\vec{R})\psi_{n\Lambda S}(\vec{r},R)\,. \tag{3}$$

The reflection and inversion symmetries of the system are not broken by the coupling, so that the

full wave function Ψ, and hence the coefficients $F_{n\Lambda S}$, may be characterized by the $\pm$ and g,u labels which appear on the adiabatic-state designations of Table I (i.e., 0_g^-, 0_u^+, etc.). The projection Ω of total electronic angular momentum on the internuclear axis is not, in general, conserved in a collision. However, in the present model, where all transitions are assumed to result from the spin-orbit interaction, the value of Ω does not change in the collision. This is simply a "J_z-conserving" approximation,[27] where $\hat{z}$ is the internuclear axis, which rotates throughout the collision. Hence, the wave function Ψ and coefficients $F_{n\Lambda S}$ can be characterized by Ω as well. Referring now to Table I, one sees that $^3P_0 \leftrightarrow {}^3P_2$ transitions occur in the $0_{g,u}^-$ "scattering symmetries," $^1P_1 \leftrightarrow {}^3P_1$ in the $0_{g,u}^+$ and $1_{g,u}$ symmetries, and $^3P_2 \leftrightarrow {}^1P_1$ or $^3P_1$ in the $1_{g,u}$ symmetries. All other transitions are "forbidden" in the framework of this model. The extent to which this limitation is physically realistic will be discussed in Sec. V.

Therefore, the coupled equations simplify to

$$[-(1/2\mu)\nabla_R^2 - \mathcal{E} + E_{n\Lambda S}(R)]F_{n\Lambda S}(\vec{R}) = -\sum_{n'\Lambda'S'} \langle n\Lambda S | V_{so} | n'\Lambda'S' \rangle F_{n'\Lambda'S'}(\vec{R}), \quad (4)$$

where the diagonal matrix elements are simply the $n\Lambda S$ adiabatic molecular energies (including nuclear repulsion), ignoring the spin-orbit interaction; the "coupling" matrix elements are approximated by retaining only the spin-orbit contribution. At large separations the expansion in terms of $\psi_{n\Lambda S}$ becomes awkward since the latter are not the correct eigenfunctions of the Hamiltonian for the dissociated system and, consequently, certain of the coupling matrix elements do not vanish as $R \to \infty$. This complication may be avoided by transforming at some large separation R_0, to the fully adiabatic representation where the basis functions $\psi_{\nu\Omega}$ are the eigenfunctions of H_e, which of course includes the spin-orbit interaction. Thus we write

$$\Psi(\vec{r},\vec{R}) = \sum_{\nu\Omega} \mathcal{F}_{\nu\Omega}(\vec{R})\psi_{\nu\Omega}(\vec{r},R), \quad (5)$$

and it is assumed that for $R \geq R_0$ all nonadiabatic coupling can be ignored. The $\mathcal{F}_{\nu\Omega}$ satisfy the simple equations

$$[-(1/2\mu)\nabla_R^2 - \mathcal{E} + E_{\nu\Omega}(R)]\mathcal{F}_{\nu\Omega}(\vec{R}) = 0, \quad (6)$$

where the diagonal matrix elements $E_{\nu\Omega}(R)$ are the fully adiabatic electronic energies (including nuclear repulsion). The actual procedure used in applying the transformation will be discussed in Sec. IV.

The matrix elements in Eqs. (4) and (6) are independent of the nuclear orientation $\hat{R}$ since coupling via ∇_R is ignored, so that a simple partial-wave decomposition of the form

$$F_\alpha(\vec{R}) = \frac{1}{R}\sum_l u_{\alpha l}(R) P_l(\cos\theta_R) \quad (7)$$

is appropriate, where the radial functions corresponding to $F_{n\Lambda S}$ of Eq. (3), for example, satisfy the N coupled differential equations (N is the total number of channels),

$$\left(\frac{d^2}{dR^2} + k_\alpha^2 - \frac{l(l+1)}{R^2}\right)u_{\alpha l}(R) = \sum_{\alpha'} U_{\alpha\alpha'}(R)u_{\alpha' l}(R), \quad (8)$$

where in this case α denotes quantum numbers n, Λ, and S, and where

$$k_\alpha^2 = 2\mu[\mathcal{E} - E_\alpha(\infty)], \quad (9)$$

and

$$U_{\alpha\alpha'}(R) = 2\mu\{\langle \alpha | V_{so} | \alpha' \rangle + [E_\alpha(R) - E_\alpha(\infty)]\delta_{\alpha\alpha'}\}. \quad (10)$$

Defining diagonal matrices

$$(\underline{k}^2)_{\alpha l,\alpha' l'} \equiv k_\alpha^2 \delta_{\alpha\alpha'}\delta_{ll'}$$

and (11)

$$(\underline{L}^2)_{\alpha l,\alpha' l'} \equiv l(l+1)\delta_{\alpha\alpha'}\delta_{ll'},$$

we rewrite Eq. (8)

$$\left(\frac{d^2}{dR^2} + \underline{k}^2 - \frac{\underline{L}^2}{R^2}\right)\underline{u}(R) = \underline{U}(R)\underline{u}(R), \quad (12)$$

where the square matrix $\underline{u}(R)$ contains N linearly independent vector solutions. In the present treatment we solve the corresponding integral equations

$$\underline{u}(R) = \underline{u}_c(R) + \int_0^\infty \underline{G}(R,R')\underline{U}(R')\underline{u}(R')\,dR', \quad (13)$$

in terms of the free-particle Green's-function matrix $\underline{G}(R,R')$ and the complementary solution $\underline{u}_c(R)$. These equations may be rewritten

$$\underline{u}(R) = \underline{G}^1(R) - \underline{G}^1(R)\int_0^R \underline{G}^2(R')\underline{U}(R')\underline{u}(R')\,dR' - \underline{G}^2(R)\int_R^\infty \underline{G}^1(R')\underline{U}(R')\underline{u}(R')\,dR', \quad (14)$$

where

$$[\underline{G}^1(R)]_{\alpha l,\alpha' l'} \equiv \begin{cases} k_\alpha R j_l(k_\alpha R)\delta_{\alpha\alpha'}\delta_{ll'} & \text{for } k^2 \geq 0 \\ k_\alpha R j_l(i|k_\alpha|R)\delta_{\alpha\alpha'}\delta_{ll'} & \text{for } k^2 < 0 \end{cases} \quad (15a)$$

and

$$[\underline{G}^2(R)]_{\alpha l,\alpha' l'} \equiv \begin{cases} Rn_l(k_\alpha R)\delta_{\alpha\alpha'}\delta_{ll'} & \text{for } k^2 \geq 0 \\ Rn_l(i|k_\alpha|R)\delta_{\alpha\alpha'}\delta_{ll'} & \text{for } k^2 < 0\,, \end{cases} \tag{15b}$$

with j_l and n_l the spherical Bessel and Neumann functions of order l. It is convenient to define the matrices $\underline{I}^1$ and $\underline{I}^2$ such that

$$\underline{u}(R) = \underline{G}^1\underline{I}^2 - \underline{G}^2\underline{I}^1\,. \tag{14'}$$

The equations are solved using a noniterative procedure,[28] as described in Sec. IV. From the asymptotic form of the $\underline{u}(R)$, the usual K, and hence S and T matrices are obtained. Transformation to the adiabatic $\nu\Omega$ representation, for example, allows us to determine the elements of the scattering matrix for transitions between pairs of molecular electronic states $\alpha \rightleftharpoons \alpha'$. The atomic inelastic cross sections are expressed in terms of these by taking proper account of the symmetries and statistical weights. The expressions are

$$\sigma(^3P_0 \to {}^3P_2) = \sum_{l\ \text{even}} \sigma_l[0_g^-(^3P_0 \to {}^3P_2)] + \sum_{l\ \text{odd}} \sigma_l[0_u^-(^3P_0 \to {}^3P_2)]\,, \tag{16}$$

$$\sigma(^3P_1 \to {}^3P_2) = \frac{2}{3}\sum_{l\ \text{even}} \sigma_l[1_g(^3P_1 \to {}^3P_2)] + \frac{2}{3}\sum_{l\ \text{odd}} \sigma_l[1_u(^3P_1 \to {}^3P_2)]\,, \tag{17}$$

$$\sigma(^1P_1 \to {}^3P_2) = \frac{2}{3}\sum_{l\ \text{even}} \sigma_l[1_g(^1P_1 \to {}^3P_2)] + \frac{2}{3}\sum_{l\ \text{odd}} \sigma_l[1_u(^1P_1 \to {}^3P_2)]\,, \tag{18}$$

and

$$\sigma(^1P_1 \to {}^3P_1) = \sum_{l\ \text{even}} \{\tfrac{1}{3}\sigma_l[0_g^+(^1P_1 \to {}^3P_1)] + \tfrac{2}{3}\sigma_l[1_g(^1P_1 \to {}^3P_1)]\} + \sum_{l\ \text{odd}} \{\tfrac{1}{3}\sigma_l[0_u^+(^1P_1 \to {}^3P_1)] + \tfrac{2}{3}\sigma_l[1_u(^1P_1 \to {}^3P_1)]\}\,, \tag{19}$$

where the individual partial cross sections are defined by

$$\sigma_l[\alpha \to \alpha'] = (\pi/k_\alpha^2)(2l+1)\,|T_{\alpha l,\alpha' l}|^2\,, \tag{20}$$

and similarly for the inverse cross sections.

IV. COMPUTATIONAL PROCEDURES

A. Scattering-state representations

In order to better illuminate the various mechanisms which lead to transitions between the atomic states and to facilitate the computational effort, we have represented the atom-atom collision equations in terms of three distinct bases of target functions. Each basis is related to any other by a unitary transformation and is usually applied only over a limited range of the radial variable R. Thus, the collision calculation is performed by outwardly propagating a solution in a particular representation to a given radius, transforming by the unitary transformation to another representation, and continuing the outward propagation of the solution in this new representation. We will review the definitions of the various bases and comment on their applicability in particular regimes.

1. ΛS basis

The ΛS basis used in Eq. (3) diagonalizes the electronic Hamiltonian *without* spin-orbit interactions. Coupling between the ΛS channels is provided by the off-diagonal elements of the spin-orbit matrix [see Eq. (4)]. Since the atomic spin-orbit interaction is used, the spin-orbit matrix elements in this representation are independent of R. The potential matrix elements in the ΛS basis as a function of R are displayed in Fig. 3(a) for the 1_u symmetry.

The ΛS basis has certain advantages in the short-range region of the potential curves and particular drawbacks in the long-range or asymptotic region. We have previously argued that the spin-orbit terms should provide the dominant coupling in the short-range region. The choice of the ΛS basis serves to explicitly segregate the spin-orbit effects from those arising from the spin-free electronic Hamiltonian, thus allowing a more systematic comparison of the various processes generated by the complete Hamiltonian. The coupling matrix elements are much smaller than the diagonal elements in the short-range region ($R \lesssim 4a_0$ for the present problem). Such a weak coupling case is generally easier to treat numerically than one in which the coupling elements are comparable to or larger than the diagonal terms. The ΛS basis in the region of close approach thus provides (a) a means of systematically identifying the various components of the collision process, and (b) a set of weakly coupled equations which can be efficiently solved. However, in the asymptotic region, this basis is fraught with problems. For one, the potential curves do not dissociate to the proper atomic limits. Also, as a result of the constant spin-orbit terms, the channels are strongly coupled even at very large distances. The latter feature greatly complicates the calculation not only through the problems which arise

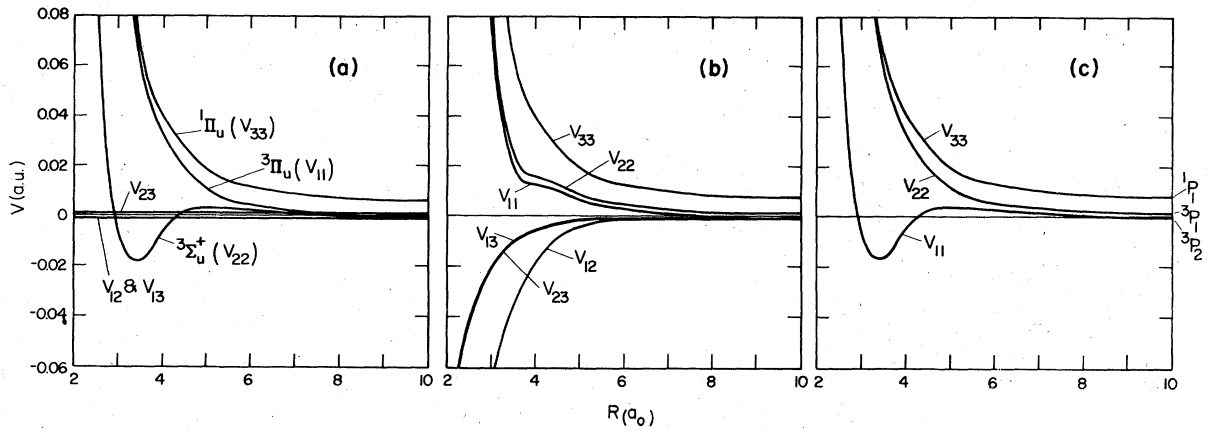

FIG. 3. Potential matrix elements in (a) the ΛS representation, (b) the transition representation (defined in the text), and (c) the Ω representation.

from strongly coupled solutions, but also from the peculiar asymptotic behavior of the scattering wave functions. Since the coupling terms do not go to zero asymptotically, the solutions do not go to the standard phase-shifted spherical plane waves for which the integral-equation codes and Green's-function routines are formulated. In order to circumvent these problems, we transform to an intermediate basis called the "transition" basis.

2. *Transition basis*

The transition basis is defined such that the potential energy curves dissociate to the proper atomic limits ($^{3,1}P_\Omega$). This basis is related to the ΛS basis by a *constant*, unitary transformation $\underline{C}$. The constant transformation is chosen so that the following matrix equation is satisfied:

$$\underline{C}^T[\underline{E}_{\Lambda S}(\infty)+\underline{V}_{so}(\infty)]\underline{C}=\underline{E}_{\nu\Omega}(\infty)\,,$$

where $(E_{\Lambda S})_{\alpha\alpha'}=E_\alpha(\infty)\delta_{\alpha\alpha'}$, $\alpha\equiv n\Lambda S$, and $(\underline{V}_{so})_{\alpha\alpha'}$ $=\langle\alpha|V_{so}|\alpha'\rangle$. In other words, the transformation is simply that which rotates the *atomic LS* basis into the *atomic* JM_J basis. This constant transformation is then applied to the ΛS basis at all values of R. The resulting potential matrix elements in the transition basis for the 1_u symmetry are displayed in Fig. 3(b).

Unlike the ΛS basis, the transition basis has distinct advantages in the intermediate to long-range region and weaknesses in the short-range region. As the separation between the atoms decreases, the coupling matrix elements in the transition basis grow rapidly. In fact, at small radii the coupling terms become comparable to or even larger than the diagonal elements. As pointed out before, such conditions of very strongly coupled channels are sometimes difficult to treat numerically. However, at larger values of R, the coupled equations become more manageable since the coupling matrix elements in this region rapidly decrease with increasing radius, tending to zero asymptotically. The solutions tend to the proper asymptotic forms of phase-shifted spherical plane waves, and the diagonal matrix elements tend to the proper atomic limits. Thus, one can use the ΛS basis to determine the solutions in the short-range region, transform to the transition basis at some intermediate radius, and continue outward propagation of the solution in this basis. However, the coupling terms do not go to zero at large R as rapidly in this basis as they do in the basis next discussed.

3. *Ω basis*

The Ω basis, used in Eq. (5), is chosen to diagonalize the electronic Hamiltonian including spin-orbit interactions. The states are coupled only by the terms arising from the nuclear motion [see Eq. (2)]. Since the spin-orbit effects are expected to provide the dominant coupling and since the nuclear coupling terms are less convenient to calculate, the Ω basis is employed only in the near-asymptotic region where these terms are negligible. The potential matrix elements in the Ω basis for the 1_u symmetry are displayed in Fig. 3(c). The Ω basis is related to the transition basis by an R-dependent unitary transformation $\underline{D}(R)$, such that $\underline{D}(R)\to 1$ as $R\to\infty$. The set of coupled equations, which ensues from transforming the transition-basis equations to the Ω basis, have coupling terms which depend on the first and second derivatives of the unitary transformation with respect to R. However, at very large radii the terms in the Ω-basis equations depending on the transformation can be neglected. The resulting

set of collision equations is completely uncoupled. The advantage of this form is that each channel solution can be outwardly integrated from the transformation radius independently of the solutions in the other channels, thus greatly reducing the computation time.

We shall briefly summarize the procedure employed for integrating the coupled integral equations. The set of coupled equations is initially referred to the ΛS basis and propagated to a radius at which the coupling is comparable to that in the transition basis. A constant unitary transformation is then performed on the wave functions, taking them from the ΛS to the transition basis. The propagation of the coupled equations in the transition basis is continued until a radius is reached at which the coupling *in the* Ω *basis* becomes negligible, where a transformation to the Ω basis is made and subsequently each decoupled channel is propagated independently to the region where the full solution can be matched to the asymptotic form of phase-shifted plane waves. Transformation between representations was carried out by first using the quadrature formula to relate $\underline{I}^2$ and $\underline{I}^1$ in Eq. (14′) at two neighboring points. The resulting pair of linear equations was then solved for $\underline{I}^2$ and $\underline{I}^1$ at the transformation point. The two transformation radii are not unique quantities, and the cross sections must be shown to be insensitive to their respective choices.

In order to verify that the coupling in the Ω basis is effectively smaller than the coupling in the transition basis at large R, we can approximate the radial momentum classically and estimate the ratio λ of the former to the latter,[7,9]

$$\lambda(R) \simeq \left(\left| k \frac{d\alpha}{dR} \right| + \frac{1}{2} \left| \frac{d^2\alpha}{dR^2} \right| \right) \Big/ \mu V^t_{12}(R) , \tag{21}$$

where $\underline{V}^t$ is the potential matrix in the transition representation (the states are labeled 1 and 2 for definiteness) and

$$\alpha(R) = \tfrac{1}{2} \tan^{-1} \frac{2V^t_{12}(R)}{V^t_{22}(R) - V^t_{11}(R)} \tag{22}$$

is the parameter of the 2×2 unitary transformation matrix connecting the different representations in a two-state approximation, which suffices for this demonstration. By differentiation of Eq. (22), it is found that

$$\frac{d\alpha}{dR} = \left((V^t_{22} - V^t_{11}) \frac{dV^t_{12}}{dR} - V^t_{12} \frac{d}{dR} (V^t_{22} - V^t_{11}) \right) \Big/ \left[(V^t_{22} - V^t_{11})^2 + 4(V^t_{12})^2 \right] . \tag{23}$$

In the case of the $Ne(^1P_1) + Ne$ and $Ne(^3P_1) + Ne$ states of 0^+_u symmetry, which are coupled by a long-range potential $-0.072/R^3$, we find (for large R)

$$\lambda \simeq (1/R)(0.9E^{1/2} + 0.05/R) , \tag{24}$$

where E is assumed in eV and R in a_0 units. The static term is negligible at all energies of interest. Hence, if the coupling in the transition basis becomes negligible at R_t, the coupling in the Ω basis becomes negligible at about

$$R_a \simeq E^{1/8} R_t^{3/4} \tag{25}$$

[in the same units as Eq. (24)]. That is, at $E = 1$ eV, transformation to the adiabatic representation, at say $R = 20a_0$, saves more than another $30a_0$ of coupled-equation integration. The integration then continues in the decoupled representation until the diagonal phases converge. This example is typical of a case involving inverse R^3 long-range coupling, where a brute-force approach may require coupled-equation integration to beyond $100a_0$. In the case of the transformation to the adiabatic representation (Ω basis), the (derivative) coupling in the new representation is neglected. This neglect normally results in a very small decrease in the symmetry of the numerical S matrix. The results obtained by transforming at $R = 20a_0$ and finishing the integration in the adiabatic representation were found to be in excellent agreement with those obtained by integrating in the transition basis all the way.

While the ΛS basis provides a more explicit representation of the various mechanisms leading to transitions than does the transition basis, we find for the present problem that, with the numerical schemes described in Sec. IV B there appears to be no distinct computational advantage in employing the ΛS rather than the transition basis in the short-range region. Therefore, in most cases the calculations were simply started in the transition basis.

B. Solution of the coupled integral equations

Whichever of the three bases is employed, the resulting set of coupled integral equations has the general form of Eq. (14). In order to solve Eq. (14) numerically, we approximate the integrals by a quadrature scheme,

$$\int_0^R f(R)\, dR \cong \sum_{i=1}^{N} f(R_i) w_i , \tag{26}$$

where N is the number of points in the quadrature and w_i is the quadrature weight for the ith point. The most extensively used quadrature[28,29] for solving the set of coupled integral equations describing collision problems is the trapezoidal rule. By using the simple trapezoidal scheme, we are generally gaining stability at the expense of accuracy. However, the T-matrix elements

for the neon-neon collisions, calculated from the asymptotic form of the channel wave functions propagated with the trapezoidal quadrature, displayed a striking departure from the usual symmetry (six to eight significant figures) obtained with the integral-equations technique. In order to more explicitly test the applicability of the quadrature, we devised a simple potential which closely modeled the principal features of the neon collision. The wave function calculated in the trapezoidal scheme for this model was found to be in poor agreement with the analytically determined solution. Even increasing the accuracy by increasing the number of points in the integration mesh failed to significantly improve the agreement. We thus considered a higher-order quadrature scheme.

Higher-order quadrature schemes, while improving the accuracy of the solution, are generally less stable than the trapezoidal rule.[30] A procedure recently proposed by Knirk,[31] in which two forms of the Simpson's quadrature were combined, showed promise for producing the highly accurate solutions of the standard two-step Simpson's rule while providing a more stable solution by incorporating a one-step rule. The wave function produced by this quadrature scheme was in excellent agreement (eight significant figures) with the analytical wave function of the model potential. We also applied the quadratic quadrature method to a number of other systems, such as electron–hydrogen-atom elastic collisions and atom-molecule rotational-excitation collisions, for which the trapezoidal rule was known to give accurate results. It yielded the same degree of accuracy using much larger step sizes, thus reducing the computation times by as much as a factor of 2. The quadratic scheme was used in all calculations of neon cross sections. Unlike the trapezoidal rule, it produced highly symmetric T matrices. In addition, the higher-order scheme produced a more accurate representation of the wave function and allowed a significant reduction in the number of mesh points.

Despite the accuracy gained from the higher-order quadrature scheme, the elements of the solution matrix in some cases tend to become linearly dependent as the wave function is outwardly propagated. This linear dependence arises from (i) the highly disparate growth of the individual channels in the short-range region, where they experience radically different potentials, and (ii) the inability (largely due to numerical round-off error of the computer) of the numerical algorithm to accurately follow the solutions. We circumvent the linear-dependence problem by placing the solution matrix in upper triangular form.[28(b)] As the solution is outwardly propagated, the triangularization procedure is regularly applied so as to guarantee the continued linear independence of the solution. We emphasize that triangularization can only maintain the integrity of a linearly independent solution and cannot salvage a solution that has become dependent. A triangularization every three steps in the classically forbidden region and every six steps in the classically allowed region was found to be sufficient to guarantee the linear independence of the solution.

Since the quadrature of the integral equation involves a large number of mesh points (a step size of $0.01a_0$ was used in most cases), a considerable fraction of the computation time is spent in calculating the Green's functions (the spherical Ricatti-Bessel functions), particularly if recurrence relations are used to obtain the functions with large l. A substantial savings was gained by using Numerov integration to propagate these functions in regions, where $k^2 - l(l+1)/R^2 > 0$, using a step size half that used in the integral-equation quadrature. Accuracy was carefully checked and there was no difference between scattering results obtained using the recurrence or Numerov techniques.

Closed channels present yet another problem in solving the set of coupled integral equations. For $k_\alpha^2 < 0$, the G^1 function in Eq. (15) has a growing exponential component which can lead to machine overflow and linear-dependence problems if the solution must be integrated to large values of R. To circumvent this problem, we scale the G^1 component of the Green's function for the closed channels by $\exp(-|k_\alpha|R)$ and the G^2 component by $\exp(|k_\alpha|R)$. Since the G^1 and G^2 components appear in the integral equations in product form evaluated at nearby mesh points, the resulting propagation scheme depends only on an exponential function $[\sim \exp(|k_\alpha|\Delta)]$ of the step size Δ. The solutions remain finite and well behaved. Another complication introduced by closed channels is that the advantage of Numerov integration of the Green's functions is lost when closed channels are included. The $\mathrm{Ne}(^1P_1)$ state is closed at scattering energies below 0.229 eV relative to $\mathrm{Ne}(^3P_2)$. When the third 1_g or 1_u state (in the transition basis) was simply left out of the calculation, the remaining $^3P_1 \rightarrow {}^3P_2$ cross section changed significantly, even when the omitted state was quite inaccessible energetically. This very surprising result was soon discovered to be misleading. When the 3×3 potential matrix was block diagonalized (by performing successive Jacobi rotations on the 1, 3 and 2, 3 elements until they converged to zero, so as to induce minimal change

in the 1,2 element), it was found that the two-state calculation was in full accord with the three-state calculation, as expected.

V. RESULTS AND DISCUSSION

The calculated cross sections[32] for the exothermic transitions $^3P_0 \rightarrow {}^3P_2$, $^3P_1 \rightarrow {}^3P_2$, $^1P_1 \rightarrow {}^3P_2$, and $^1P_1 \rightarrow {}^3P_1$ are illustrated in Figs. 4–7, respectively. Contributions from the different molecular symmetries are shown as well as the observable totals. Numerical values for each contribution are listed in Table II. A characteristic feature of all of these cross sections is a steep rise in magnitude with increasing energy. This behavior results from the repulsive nature of the potential curves at intermediate and large separations, but still inside the Van der Waals minima (see Figs. 1 and 2). The $^1\Sigma_u^+$ and $^3\Sigma_u^+$ curves, and consequently the $0_u^-(^3P_2)$, $0_u^+(^3P_1)$, and $1_u(^3P_2)$ curves, do possess deep minima around $R = 3.5a_0$, but each curve exhibits a potential "hump" at larger separations. The magnitudes of these potential maxima for the $^3\Sigma_u^+$ and $^1\Sigma_u^+$ curves are 0.087 eV (at $R = 5.4a_0$) and 0.064 eV (at $R = 5.5a_0$), respectively. Corresponding potential maxima in the $0_u^-(^3P_2)$, $0_u^+(^3P_1)$, and $1_u(^3P_2)$ curves are 0.107 eV (at $R = 4.9a_0$), 0.198 eV (at $R = 4.8a_0$), and 0.108 eV (at $R = 4.9a_0$), respectively. The $0_u^+(^1P_1)$ curve has a shallow minimum and a potential maximum of the order 0.06 eV.

The relative contributions of different molecular symmetries to the inelastic cross sections vary with energy in a way that can be understood mainly

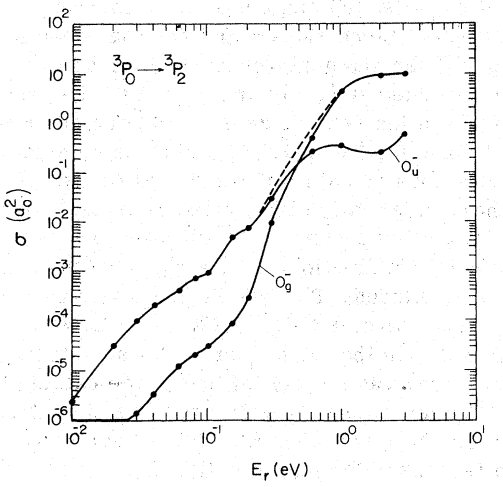

FIG. 4. Cross section for $Ne(^3P_0) + Ne(^1S) \rightarrow Ne(^3P_2) + Ne(^1S)$ (dashed curve) as a function of collision energy. The contributions from the various molecular symmetries are also shown (the data points indicate where close-coupling calculations were actually performed).

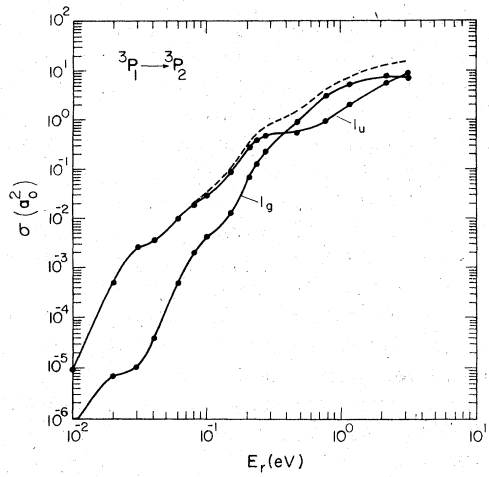

FIG. 5. Contributions to the cross section for $Ne(^3P_1) + Ne(^1S) \rightarrow Ne(^3P_2) + Ne(^1S)$ as a function of collision energy. The dashed curve is the total cross section.

in terms of the *adiabatic* potential curves of Figs. 2(a) and 2(b). Even though we do not actually compute the cross sections using the adiabatic ($\nu\Omega$) representation, except in the asymptotic region, nevertheless it is useful to refer to these curves in interpreting the results. At low energies, the coupling is weak, so that the quantum trajectories of the atoms are largely determined by the adiabatic ($\nu\Omega$) potential energies.

In the case of the $^3P_0 \rightarrow {}^3P_2$ transition, for example, we see from Fig. 4 that the 0_u^- contribution dominates at low energies, but gives way to 0_g^- above about 0.5 eV. In Fig. 2(a), we see that the $0_u^-(^3P_0)$ curve rises less rapidly than the $0_g^-(^3P_0)$ curve and remains below it as R is decreased

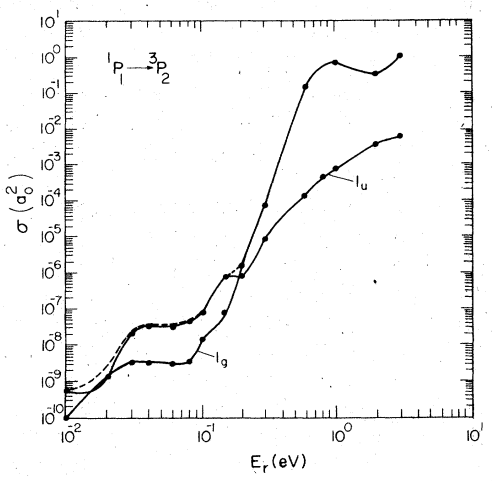

FIG. 6. Contributions to the cross section for $Ne(^1P_1) + Ne(^1S) \rightarrow Ne(^3P_2) + Ne(^1S)$ as a function of collision energy. The dashed curve is the total cross section.

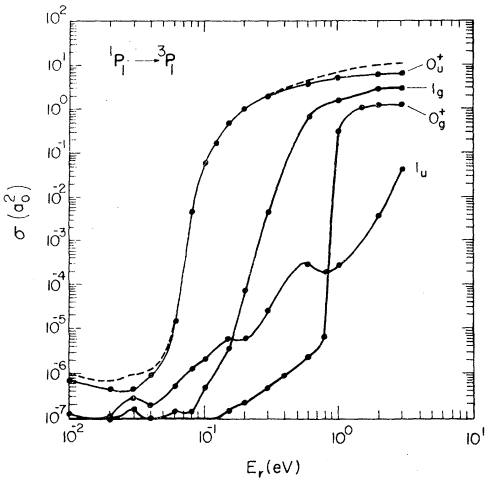

FIG. 7. Contributions to the cross section for $Ne(^1P_1) + Ne(^1S) \rightarrow Ne(^3P_1) + Ne(^1S)$ as a function of collision energy. The dashed curve is the total cross section.

from say $6.5a_0$ to $5a_0$. Thus, for incident energies (c.m.) of less than 0.3 eV or so, the classical turning point for the $0_u^-(^3P_0)$ trajectory will lie well inside that for the $0_g^-(^3P_0)$ trajectory. Since at these separations the coupling between the states is comparable and increases with decreasing R, the 0_u^- contribution to the $^3P_0 \rightarrow {}^3P_2$ cross section is understandably larger. As the energy is increased the steep rise in the 0_u^- curve is felt in two ways: the classical turning points shift outside those corresponding to the 0_g^- curve, and the energy separation of the $0_u^-(^3P_0)$ and $0_u^-(^3P_2)$ curves become significantly larger than that between the corresponding 0_g^- curves. Both effects favor a larger relative 0_g^- contribution at higher energies. Similar arguments apply to the $^3P_1 \rightarrow {}^3P_2$ transition, where the relevant symmetries are 1_g and 1_u.

In the case of the $^1P_1 \rightarrow {}^3P_2$ transition, the 1_u symmetry again dominates at energies in the range $0.03\ \text{eV} \lesssim E \lesssim 0.15\ \text{eV}$. However, a casual glance at the potential curves suggests that it should be the other way around. The $1_u(^1P_1)$ curve rises more steeply than the $1_g(^1P_1)$ curve and remains above it at all R. Similarly, the energy separation of the $1_u(^1P_1)$ and $1_u(^3P_2)$ curves at small R is much larger than that of the corresponding 1_g curves. In this case it turns out that the coupling matrix element (in the "transition

TABLE II. Calculated Ne*+Ne inelastic cross sections (power of ten given in parentheses).

	$^3P_0 \rightarrow {}^3P_2$	$^3P_0 \rightarrow {}^3P_2$	$^1P_1 \rightarrow {}^3P_1$	$^1P_1 \rightarrow {}^3P_1$	$^1P_1 \rightarrow {}^3P_1$	$^1P_1 \rightarrow {}^3P_1$	$^3P_1 \rightarrow {}^3P_2$	$^3P_1 \rightarrow {}^3P_2$	$^1P_1 \rightarrow {}^3P_2$	$^1P_1 \rightarrow {}^3P_2$
E_r (eV)	0_u^-	0_g^-	0_u^+	0_g^+	1_u	1_g	1_u	1_g	1_u	1_g
0.010	2.47(−6)	2.92(−8)	2.13(−6)	3.70(−7)	1.16(−7)	1.26(−7)	1.41(−5)	7.10(−7)	8.04(−10)	1.48(−10)
0.020	3.15(−5)	4.53(−7)	1.36(−6)	2.36(−7)	1.66(−7)	5.16(−8)	7.57(−4)	1.06(−5)	1.99(−9)	2.02(−9)
0.030	9.82(−5)	1.42(−6)	1.37(−6)	1.42(−7)	4.53(−7)	2.53(−7)	3.85(−3)	1.53(−5)	2.99(−8)	4.97(−9)
0.040	2.01(−4)	3.37(−6)	2.85(−6)	1.11(−7)	3.07(−7)	7.26(−8)	5.33(−3)	5.91(−5)	5.12(−8)	4.96(−9)
0.060	4.15(−4)	1.15(−5)	4.59(−5)	2.06(−7)	7.97(−7)	2.18(−7)	1.55(−2)	7.38(−4)	4.78(−8)	4.34(−9)
0.080	7.48(−4)	2.05(−5)	1.45(−2)	1.25(−7)	1.99(−6)	2.19(−7)	2.90(−2)	2.98(−3)	6.80(−8)	5.29(−9)
0.100	9.44(−4)	3.10(−5)	1.83(−1)	1.55(−7)	3.22(−6)	7.20(−7)	4.54(−2)	6.24(−3)	1.22(−7)	2.17(−8)
0.120			5.16(−1)							
0.150	4.85(−3)	8.49(−5)	1.47(0)	4.69(−7)	8.89(−6)	5.83(−6)	1.34(−1)	2.00(−2)	1.13(−6)	1.09(−7)
0.200	7.66(−3)	2.82(−4)	3.13(0)	6.93(−7)	9.00(−6)	1.17(−4)			1.22(−6)	2.30(−6)
0.207							4.26(−1)	1.04(−1)		
0.237							5.90(−1)	1.95(−1)		
0.277							7.20(−1)	3.61(−1)		
0.300	3.09(−2)	9.72(−3)	6.02(0)	1.48(−6)	3.85(−5)	6.91(−3)			1.40(−5)	1.19(−4)
0.400				2.72(−6)						
0.477							8.72(−1)	1.37(0)		
0.500				5.00(−6)						
0.600	2.78(−1)	5.26(−1)	1.11(+1)	7.81(−6)	4.50(−4)	1.06(0)			2.25(−4)	2.48(−1)
0.777							1.44(0)	4.83(0)		
0.800				2.01(−5)	2.77(−4)				6.93(−4)	
1.000	3.72(−1)	4.50(0)	1.52(+1)	9.89(−1)	4.03(−4)	2.38(0)			1.16(−3)	1.13(0)
1.177							3.08(0)	8.08(0)		
1.200				2.50(0)						
1.500				3.25(0)						
2.000	2.71(−1)	9.77(0)	1.88(+1)	3.84(0)	5.84(−3)	4.46(0)			6.17(−3)	5.58(−1)
2.177							8.37(0)	1.16(+1)		
3.000	6.18(−1)	1.02(+1)	2.01(+1)	3.86(0)	6.75(−2)	4.76(0)			9.91(−3)	1.62(0)
3.177							1.32(+1)	1.07(+1)		

representation," for example) is simply larger for the 1_u symmetry, resulting in the larger cross section. At the higher energies, however, the other effects are more important.

The $^1P_1 \rightarrow {}^3P_1$ cross section is dominated by the 0_u^+ contribution at all energies and exhibits a rapid rise between 0.05 and 0.10 eV. An avoided crossing between the $0_u^+(^1P_1)$ and $0_u^+(^3P_1)$ curves, which becomes accessible at incident energies near 0.07 eV, plays an important role here. This feature is evident as a curve crossing between the $^1\Sigma_u^+(^1P)$ and $^3\Pi_u(^3P)$ curves in the $n\Lambda S$ representation; the crossing is removed by the spin-orbit interaction. The qualitative features of the 0_u^+ contribution to the $^1P_1 \rightarrow {}^3P_1$ cross section are evident in a Landau-Zener (LZ) cross section, calculated in the transition representation, which only allows transitions at the curve crossing.[33] The LZ and close-coupling results are compared in Fig. 8(a) for the 0_u^+ states. The 0_g^+ states contribute essentially nothing to the $^1P_1 \rightarrow {}^3P_1$ cross section at collision energies below 1 eV, but at higher energies a crossing in this pair of curves becomes accessible. The LZ contribution resulting from this crossing is shown in Fig. 8(b). The LZ approximation is not too bad for these curve crossing cases at the highest collision energies evaluated by close coupling and hence might reasonably be used to extrapolate to somewhat higher energies, e.g., to determine the energy at which the cross section is maximum. In Figs. 9(a)–9(c) the individual partial-wave distributions corresponding to the 0_u^+ close-coupling calculations are compared with the LZ results at the three incident energies $E = 0.1$, 0.3, and 1.0 eV. In the LZ calculation, no attempt was made to recover the oscillations resulting from the difference in the phases of the initial and final trajectories; only the envelope is presented. Returning to the integrated cross-section calculations, we note that 1_u is by far the least important of the remaining contributions, presumably owing to the steep, repulsive nature of the $1_u(^3P_1)$ potential curve. The rapid onset of the 0_g^+ contribution results from surmounting the hump in the $0_g^+(^1P_1)$ curve and reaching the avoided crossing between the pair of 0_g^+ curves at about 1 eV. This is better illustrated by the change in partial-wave distribution as the energy is increased to exceed the barrier height. In Figs. 10(a) and 10(b) the partial-wave distributions are shown for the 0_g^+ cross section at the two energies $E = 0.3$ and 1.0 eV (relative to the $^1P_1$ state). The shift, as the energy is pushed over the 0_g^+ barrier, from a situation where one obtains very small contributions over a large range of l to that where the main contributions arise from a small number of partial waves with $l < 50$ is evident.

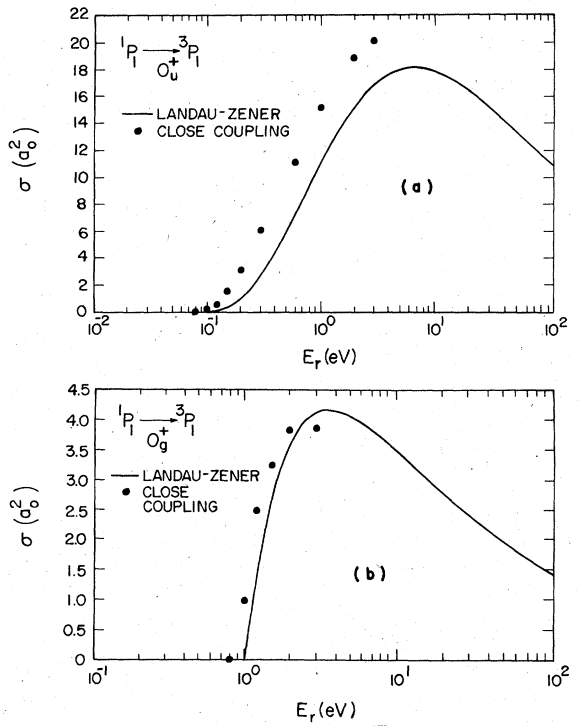

FIG. 8. Comparison of the Landau-Zener cross sections (with parameters corresponding to the matrix elements in the transition representation) to the close-coupling results for the $Ne(^1P_1) + Ne(^1S) \rightarrow Ne(^3P_1) + Ne(^1S)$ collision with (a) 0_u^+ and (b) 0_g^+ symmetry. The LZ thresholds are 0.068 and 0.99 eV, respectively.

The experimental determination of these cross sections is difficult and only a few measurements have been made. These are swarm experiments and only the rate coefficients for a particular velocity distribution are obtained. In order to compare with the experimental data, we have presented, in Table III, deexcitation rate constants $K = \langle v\sigma \rangle$, where the average is taken over a Maxwell-Boltzmann velocity distribution for a variety of temperatures. The average cross section $\bar{\sigma}$ is defined by

$$\bar{\sigma} = K/\bar{v}\,, \tag{27}$$

where $\bar{v}$ is the mean speed.

In Fig. 11 the theoretical rates for the $^3P_1 \rightarrow {}^3P_2$ transition are compared with several existing measurements.[34-37] The agreement at the higher temperatures is encouraging. One possible explanation of the deviation at temperatures below 300 °K is that the theoretical $1_u(^3P_1)$ potential energy curve may be slightly too repulsive at large separations. The low-energy cross sections are, indeed, very sensitive to small changes in the potential curve corresponding to the initial state. An accurate theoretical determination of the cross

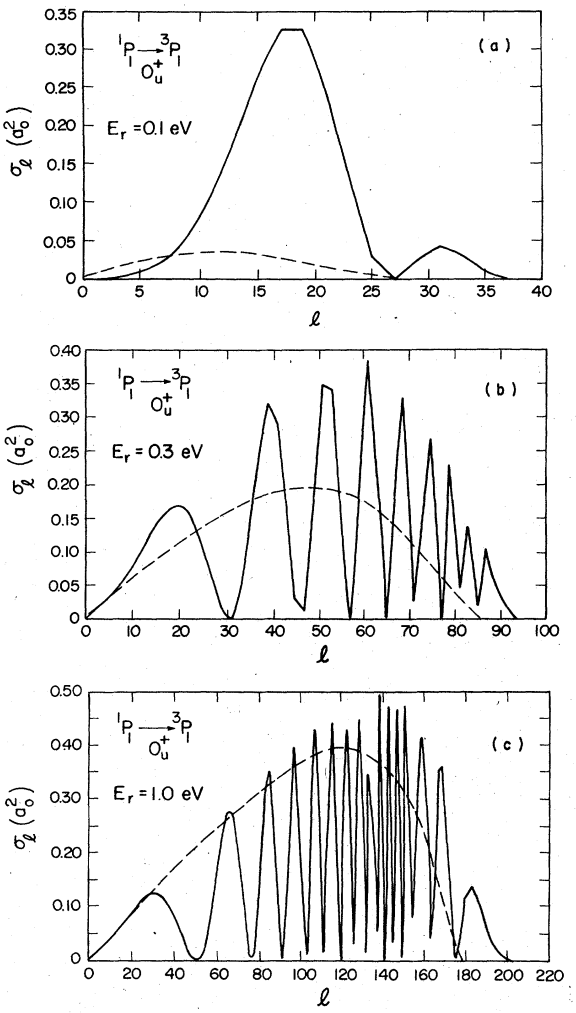

FIG. 9. Partial cross sections for $Ne(^1P_1)+Ne(^1S) \rightarrow Ne(^3P_1)+Ne(^1S)$ in 0_u^+ symmetry at incident relative energies of (a) 0.1 eV, (b) 0.3 eV, and (c) 1.0 eV. The Landau-Zener *envelope* (i.e., not multiplied by a phase factor which is always less than or equal to unity) is shown as a dashed curve.

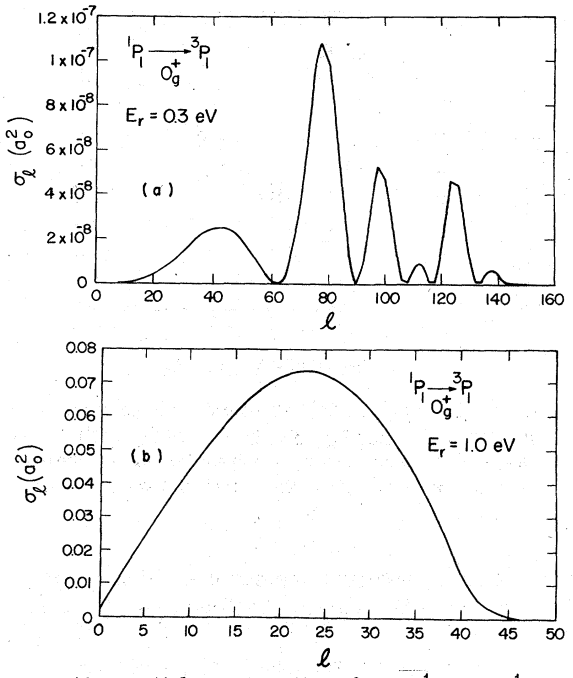

FIG. 10. Partial cross sections for $Ne(^1P_1)+Ne(^1S) \rightarrow Ne(^3P_1)+Ne(^1S)$ in 0_g^+ symmetry at incident relative energies of (a) 0.3 eV and (b) 1.0 eV.

sections at this end may require a more accurate potential curve. Another possible explanation is discussed below.

The $^3P_0 \rightarrow {}^3P_2$ rate has also been measured at 300 °K, but the temperature dependence has not yet been experimentally determined.[36] The experimental value is of the order 5×10^{-15} cm^3/sec at 300 °K. Our theoretical value given in Table III is 1.3×10^{-15} cm^3/sec. Again, this may suggest that the $0_u^-(^3P_0)$ potential energy curve is slightly too repulsive at large separations. However, since the low-temperature rate and average cross section are so small, we cannot rule out the possibility that the nonadiabatic "rotational" (or "Coriolis") coupling terms, ignored in the present model, are significant here and indeed might even dominate the room-temperature rates. We predict a strong temperature dependence for this transition with the theoretical rate and average cross section increasing by an order of magnitude as the temperature is increased from 300 to 600

TABLE III. Rate constants for Ne*+Ne inelastic collisions.[a]

	K (cm^3/sec)[b]			
T (°K)	$^3P_0 \rightarrow {}^3P_2$	$^1P_1 \rightarrow {}^3P_1$	$^3P_1 \rightarrow {}^3P_2$	$^1P_1 \rightarrow {}^3P_2$
100	5.8×10^{-17}	4.3×10^{-17}	1.2×10^{-15}	9.5×10^{-21}
200	3.9×10^{-16}	9.2×10^{-15}	9.6×10^{-15}	4.9×10^{-20}
300	1.3×10^{-15}	7.6×10^{-14}	3.5×10^{-14}	3.6×10^{-19}
400	3.3×10^{-15}	2.4×10^{-13}	8.9×10^{-14}	5.7×10^{-18}
600	1.6×10^{-14}	9.4×10^{-13}	3.3×10^{-13}	3.4×10^{-16}
800	5.8×10^{-14}	2.0×10^{-12}	7.5×10^{-13}	3.8×10^{-15}
1000	1.6×10^{-13}	3.5×10^{-12}	1.3×10^{-12}	1.7×10^{-14}
1500	9.4×10^{-13}	7.7×10^{-12}	3.3×10^{-12}	1.2×10^{-13}
2000	2.6×10^{-12}	1.3×10^{-11}	7.0×10^{-12}	4.2×10^{-13}
2500	5.4×10^{-12}	1.9×10^{-11}	1.2×10^{-11}	1.1×10^{-12}
3000	9.8×10^{-12}	2.4×10^{-11}	1.7×10^{-11}	1.5×10^{-12}

[a] For a Maxwellian distribution.

[b] The inverse rate constants can be obtained as follows: $K(^3P_2 \rightarrow {}^3P_0) = 0.2\exp(-1118/T)K(^3P_0 \rightarrow {}^3P_2)$, $K(^3P_1 \rightarrow {}^1P_1) = \exp(-2057/T)K(^1P_1 \rightarrow {}^3P_1)$, $K(^3P_2 \rightarrow {}^3P_1) = 0.6\exp(-601/T)K(^3P_1 \rightarrow {}^3P_2)$, $K(^3P_2 \rightarrow {}^1P_1) = 0.6\times\exp(-2657/T)K(^1P_1 \rightarrow {}^3P_2)$.

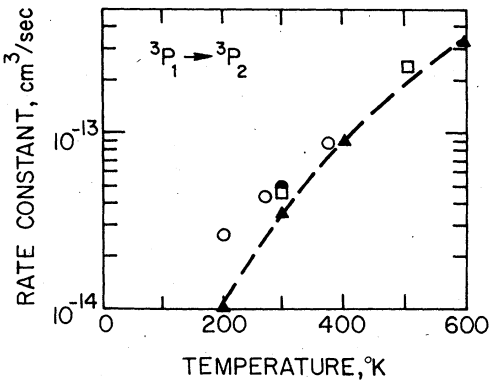

FIG. 11. Comparison of theoretical and experimental rate constants for $Ne(^3P_1) + Ne(^1S) \rightarrow Ne(^3P_2) + Ne(^1S)$. Theoretical: ▲ present results; experimental: □ Phelps (Ref. 36); ○ Grant and Krumbein (Ref. 34); ● Leichner *et al.* (Ref. 37).

°K. Measurements at temperatures higher than 300 °K would be helpful in checking these predictions.

The $^3P_0 \rightarrow {}^3P_1$ cross section is identically zero in the present theoretical model. The $\nu\Omega$ molecular states arising from $^3P_0$ are 0_u^- and 0_g^-, and these do not couple (via the spin-orbit interaction) with the 0_u^+, 0_g^+, 1_u, and 1_g states which correlate to the $^3P_1$ atomic state. We are not suggesting that the cross section is actually zero, only that it is small. A proper treatment of the rotational coupling would couple $0_u^-(^3P_0)$ with $1_u(^3P_2)$ and $0_g^-(^3P_0)$ with $1_g(^3P_2)$ resulting in a nonzero cross section. Phelps[36] reports an experimental value of the average cross section for this transition of 6×10^{-20} cm^2, the same as for the $^3P_0 \rightarrow {}^3P_2$ transition. Such a near equality might be expected if rotational coupling dominates the cross section, since the $\Omega = 1$ curves from the two states contain about equal parts of $^3\Sigma$ and $^3\Pi$ character which can be coupled to the $^3\Pi$ and $^3\Sigma$ parts, respectively, of the 0^- curves. If this explanation is correct we would predict a somewhat larger difference in these two cross sections for the heavier rare gases (Ar, Kr, and Xe) where there is considerably more singlet character mixed into the $1_{g,u}(^3P_1)$ states. In any event, we expect the spin-orbit coupling to dominate rotational coupling at higher scattering energies ($\gtrsim$0.2 eV). Work on the rotational coupling contributions will continue.

The $^1P_1 \rightarrow {}^3P_1$ deexcitation rate has been measured by Leichner *et al.*[37] who obtain the value 5.5×10^4 sec^{-1}/Torr (1.7×10^{-12} cm^3/sec) at 300 °K; this corresponds roughly to an average cross section of 2×10^{-17} cm^2. This is over an order of magnitude larger than our theoretical value and, in fact, is in agreement with our result at about 750 °K. It is probably true that our cross section and corresponding rate are too small at low energies for essentially the same reasons as given previously, in connection with the $^3P_1 \rightarrow {}^3P_2$ cross sections. However, based in part on the good agreement with Phelps for the latter transition above 400 °K, this discrepancy is somewhat larger than we would have expected.

ACKNOWLEDGMENTS

This work was supported in part by the U.S. Department of Energy, the Office of Energy Research, and by the Robert A. Welch Foundation. One of the authors (N. F. L.) would like to express his appreciation to the staff of the Joint Institute for Laboratory Astrophysics, University of Colorado and National Bureau of Standards, Boulder, Colorado, where a portion of this work was completed.

*Present address: Theoretical Division, Los Alamos Scientific Laboratory, Univ. of California, Los Alamos, N.M. 87545.

[1]H. S. W. Massey, *Electronic and Ionic Impact Phenomena: Slow Collisions of Heavy Particles* (Oxford U.P., London, 1971), Vol. III, Chap. 18, p. 1651.

[2]H. S. W. Massey and H. B. Gilbody, *Electronic and Ionic Impact Phenomena: Recombination and Fast Collisions of Heavy Particles* (Oxford U.P., London, 1974), Vol. IV, p. 2786.

[3]N. F. Mott and H. S. W. Massey, *The Theory of Atomic Collisions*, 3rd ed. (Oxford U. P., London, 1965), p. 665.

[4]Reference 1, p. 1914.

[5]D. R. Bates, Proc. R. Soc. A 257, 22 (1960).

[6]A. Russek, Phys. Rev. A 4, 1918 (1971).

[7]F. T. Smith, Phys. Rev. 179, 111 (1969).

[8]J. B. Delos and W. R. Thorson, Phys. Rev. Lett. 28, 647 (1972); Phys. Rev. A 6, 728 (1972); W. R. Thorson, J. B. Delos, and S. A. Boorstein, *ibid.* 4, 1052 (1971); J. B. Delos, W. R. Thorson, and S. K. Knudson, *ibid.* 6, 709 (1972); J. B. Delos, *ibid.* 9, 1626 (1974).

[9]J. S. Cohen, S. A. Evans, and N. F. Lane, Phys. Rev. A 4, 2248 (1971); S. A. Evans, J. S. Cohen, and N. F. Lane, *ibid.* 4, 2235 (1971).

[10]M. Barat and W. Lichten, Phys. Rev. A 6, 211 (1972).

[11]T. F. O'Malley, Phys. Rev. 162, 98 (1967); Adv. At. Mol. Phys. 7, 223 (1971).

[12]H. Gabriel and K. Taulbjerg, Phys. Rev. A 10, 741 (1974).

[13]D. R. Bates and R. McCarroll, Proc. R. Soc. A 245,

175 (1958); S. B. Schneiderman and A. Russek, Phys. Rev. 181, 311 (1969); M. E. Riley and T. A. Green, Phys. Rev. A 4, 619 (1971); S. K. Knudson and W. R. Thorson, Can. J. Phys. 48, 313 (1970); G. J. Hatton, J. C. Y. Chen, T. Ishihara, and K. M. Watson, Phys. Rev. A 12, 1281 (1975).

[14]G. J. Hatton, Phys. Rev. A 14, 901 (1976); G. J. Hatton, W. Lichten, and N. Ostrove, Chem. Phys. Lett. 40, 437 (1976).

[15]See, for example, E. J. Shipsey, J. C. Browne, and R. E. Olson, Phys. Rev. A 11, 1334 (1975); L. Lenamon, J. C. Browne, and R. E. Olson, *ibid.* 8, 2380 (1973); R. E. Olson, R. Morgenstern, D. C. Lorents, J. C. Browne, and L. Lenamon, *ibid.* 8, 2387 (1973).

[16]See, for example, R. A. Gutcheck, R. M. Hill, D. C. Lorents, D. L. Huestis, M. V. McCusker, and H. H. Nakano, J. Appl. Phys. 46, 3106 (1975); D. C. Lorents, Physica 82C, 19 (1976).

[17]R. E. Gleason, Jr., T. D. Bonifield, J. W. Keto, and G. K. Walters, J. Chem. Phys. 66, 1589 (1977); J. W. Keto, R. E. Gleason, Jr., T. D. Bonifield, and G. K. Walters, Chem. Phys. Lett. 42, 125 (1976); J. W. Keto, R. E. Gleason, Jr., and G. K. Walters, Phys. Rev. Lett. 33, 1365 (1974).

[18]P. K. Leichner, K. F. Palmer, J. D. Cook, and M. Thieneman, Phys. Rev. A 13, 1787 (1976); P. K. Leichner and R. J. Ericson, *ibid.* 9, 251 (1974); P. K. Leichner, *ibid.* 8 815 (1973); N. Thonnard and G. S. Hurst, *ibid.* 5, 1110 (1972); T. Oka, K. V. S. Rama Rao, J. L. Redpath, and R. F. Firestone, J. Chem. Phys. 61, 4740 (1974); W. M. Hughes, "Molecular Krypton Kinetics," in *Electronic Transition Lasers II*, edited by L. E. Wilson, S. N. Suchard, and J. I. Steinfeld (MIT, Cambridge, Mass., 1977), p. 81.

[19]J. S. Cohen and B. Schneider, Phys.Rev. A 11, 884 (1975); see related experimental paper of G. Spiess, K. T. Gillen, and R. P. Saxon, J. Phys. B 10, 899 (1977).

[20]J. S. Cohen and B. Schneider, J. Chem. Phys. 61, 3230 (1974).

[21]R. S. Mulliken, J. Chem. Phys. 52, 5170 (1970).

[22]B. Schneider and J. S. Cohen, J. Chem. Phys. 61, 3240 (1974).

[23]D. R. Bates, H. S. W. Massey, and A. L. Stewart, Proc. R. Soc. A 216, 437 (1953).

[24]We denote all electronic coordinates collectively by $\vec{r}$. The internuclear separation is denoted by R.

[25]The total wave function should include nuclear-spin functions and exhibit even or odd symmetry with respect to nuclear exchange. These spin and symmetry effects are not expected to be important at the energies considered here, and are left implicit in the formal discussion of this section.

[26]Electron-translation factors are expected to be unimportant in the present case, and are therefore ignored.

[27]R. T Pack, J. Chem. Phys. 60, 633 (1974); P. McGuire and D. J. Kouri, *ibid.* 60, 2488 (1974).

[28]W. N. Sams and D. J. Kouri, J. Chem. Phys. 51, 4815 (1969); E. F. Hayes, C. A. Wells, and D. J. Kouri, Phys. Rev. A 4, 1017 (1971).

[29]E. R. Smith and R. J. W. Henry, Phys. Rev. A 7, 1585 (1973); L. A. Collins and N. F. Lane, *ibid.* 14, 1358 (1976); D. L. Knirk, J. Chem. Phys. 57, 4782 (1972); M. A. Morrison, N. F. Lane, and L. A. Collins, Phys. Rev. A 15, 2186 (1977).

[30]D. Secrest, Methods Comput. Phys. 10, 243 (1971).

[31]D. L. Knirk, J. Comp. Phys. 21, 371 (1976).

[32]A preliminary account of these results was given by J. S. Cohen, L. A. Collins, and N. F. Lane, *Ninth International Conference on the Physics of Electronic and Atomic Collisions, Abstracts* (Univ. of Washington, Seattle, 1975), Vol. 1, p. 532.

[33]It is perhaps worth noting that the LZ approximation applied in the "transition representation" gave results in much better agreement with our close-coupling calculations than did the LZ approximation applied in the $n\Lambda S$ representation.

[34]F. A. Grant and A. D. Krumbein, Phys. Rev. 90, 59 (1953).

[35]A. V. Phelps and J. P. Molnar, Phys. Rev. 89, 1202 (1953).

[36]A. V. Phelps, Phys. Rev. 114, 1011 (1959); see also P. A. Ricard, J. Phys. (Paris) 30, 556 (1969); A. Bouvier, A. Bouvier, and J. Janin, *ibid.* 31, 957 (1970).

[37]P. K. Leichner, J. D. Cook, and S. J. Luerman, Phys. Rev. A 12, 2501 (1975); P. K. Leichner, *ibid.* 8, 815 (1973).